J|A|C|S
ARTICLES
Published on Web 04/19/2007

Janus Discs

Andreas Walther,*,† Xavier André,† Markus Drechsler,† Volker Abetz,‡ and Axel H. E. Müller*,†

Contribution from the Makromolekulare Chemie II and Bayreuther Zentrum für Kolloide und Grenzflächen, Universität Bayreuth, D-95440 Bayreuth, Germany, and ‡Institut für Polymerforschung, GKSS-Forschungszentrum Geesthacht GmbH, D-21502 Geesthacht, Germany

Received November 14, 2006; E-mail: Andreas.Walther@uni-bayreuth.de; Axel.Mueller@uni-bayreuth.de

Abstract: We describe the synthesis and the solution properties of sheet- and disclike Janus particles, containing an inner crosslinked polybutadiene (PB) layer and two different outer sides of polystyrene (PS) and poly(*tert*-butyl methacrylate) (P*t*BMA). The structures formed upon adsorption of the flat Janus particles onto solid substrates as well as in THF solution are investigated. The Janus discs are obtained in a template-assisted synthetic pathway followed by sonication. Selectively crosslinking the lamellar PB domains in a well-ordered lamellar microphase-separated bulk morphology of PS-*block*-PB-*block*-P*t*BMA (SBT) block terpolymers leads to the conservation of the compartmentalization of the two outer blocks. Sonication of the crosslinked block terpolymer templates renders soluble sheet- and disclike Janus particles, the size of which can be tuned from the micrometer range down to the nanometer scale. Small-angle X-ray scattering, transmission electron microscopy, dynamic light scattering, scanning force microscopy, and scanning electron microscopy are used to characterize the template-assisted synthetic process and the solution properties. Cryogenic transmission electron microscopy in THF and TEM of particles, embedded into a photo-crosslinkable silicon oil, indicate a supramolecular aggregation behavior of the Janus discs in concentrated solutions. Pendant drop tensiometry demonstrates that Janus sheets and discs can be used to stabilize liquid−liquid interfaces, rendering these materials interesting for future applications.

1. Introduction

In recent years, Janus particles have attracted much attention in nanoscience due to their interesting properties, for academic as well as for technological reasons.[1−8] In general, Janus structures can be divided into three classes according to their architecture: spherical Janus micelles (3D), two types of Janus cylinders (1D), and Janus sheets or discs (2D), representing the intermediate case of dimensionality (see Scheme 1). The synthesis of such non-centrosymmetric structures with compartmentalized coronas is a demanding task for the synthetic chemist. Hence, only a few real nanosized polymer-based Janus structures are known in literature.

One of the most intensively studied systems is the one concerning the spherical Janus micelles, which are based on template-assisted synthesis using polystyrene-*block*-polybutadiene-*block*-poly(methyl methacrylate) (SBM) block terpolymers. The SBM Janus micelles, as well as their amphiphilic pendants, the hydrolyzed SBMA Janus micelles (MA: methacrylic acid), show interesting hierarchical organization on different length scales. The SBM micelles form larger aggregates in nonselective organic solvents, on a silicon surface[9] and at the air/water interface.[10] The amphiphilic SBMA micelles,

Scheme 1. Possible Janus Architectures with Phase-Segregated Shells[a]

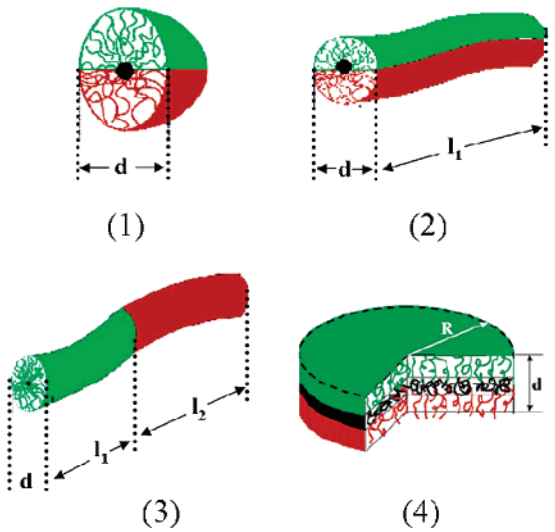

[a] (1) Janus sphere, (2, 3) two types of Janus cylinders, (4) Janus disc.

† Universität Bayreuth.
‡ Institut für Polymerforschung.

(1) Nonomura, Y.; Komura, S.; Tsujii, K. *Langmuir* **2004**, *20* (26), 11821−11823.
(2) Binks, B. P.; Fletcher, P. D. I. *Langmuir* **2001**, *17* (16), 4708−4710.
(3) Cates, M. E.; Poon, W. C. K.; Clegg, P. S.; Egelhaaf, S. U. 2005-GB2577, 2006003403, 20050701, 2006.
(4) Vanakaras, A. G. *Langmuir* **2006**, *22* (1), 88−93.
(5) Roh, K. H.; Martin, D. C.; Lahann, J. *Nat. Mater.* **2005**, *4* (10), 759−763.
(6) Perro, A.; Reculusa, S.; Ravaine, S.; Bourgeat-Lami, E.; Duguet, E. *J. Mater. Chem.* **2005**, *15* (35−36), 3745−3760.
(7) Li, Z.; Lee, D.; Rubner, M. F.; Cohen, R. E. *Macromolecules* **2005**, *38* (19), 7876−7879.
(8) Shepherd, R. F.; Conrad, J. C.; Rhodes, S. K.; Link, D. R.; Marquez, M.; Weitz, D. A.; Lewis, J. A. *Langmuir* **2006**, *22*, 8618−8622.

Scheme 2. Schematic Synthesis of Janus Discs, Based on the Selective Crosslinking of PB Domains of an SBT Terpolymer with Lamella−Lamella (ll) Morphology

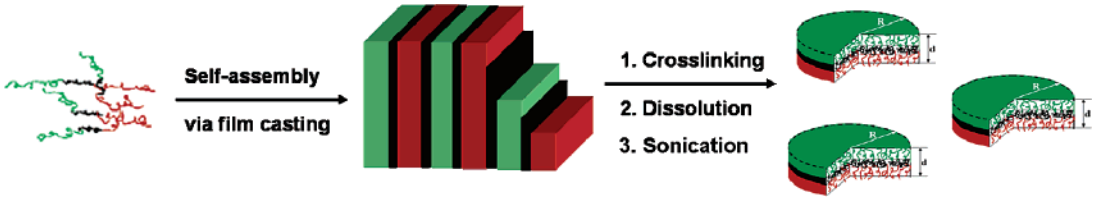

obtained after hydrolysis of the PMMA ester groups, also exhibit superstructures and giant particles.[11]

In addition, great efforts have been undertaken to obtain spherical Janus particles from heteroarm starpolymers or by using the self-assembly of block terpolymers and heteroarm star polymers in solution.[12,13] Another self-assembly approach is based on the electrostatic interactions of AB and CD diblock copolymers where B and C form insoluble complexes, e.g., interpolyelectrolyte complexes, in a solvent for blocks A and D. The first reported attempt has led to vesicles with an asymmetric wall rather than to Janus spheres.[14] Voets et al.[15] recently reported the formation of complex-coacervate core micelles with an asymmetric corona and a slightly anisometric shape. One major drawback of all of these approaches is the fact that the structures need to undergo micropohase segregation of the corona in solution. Consequently, the compartmentalization is not predestined by the template as it is the case for the template-assisted synthesis as presented herein.

Concerning nonspherical nanoscopic Janus architectures the literature is limited to very few examples. For instance, Ishizu et al.[16] synthesized amphiphilic brush-*block*-brush AB-type polymer brushes by a combined grafting-through and grafting-from process. After polymerizing a PEO macromonomer via ATRP, a second monomer (2-hydroxyethyl methacrylate, HEMA) was added to form the second block. Subsequent esterification with an ATRP initiator and an additional ATRP of HEMA rendered a Janus type polymer brush with PEO and PHEMA side chains. The polymer brush showed an ellipsoidal shape rather than a cylindrical one, as the degree of polymerization of the backbone was relatively low. A successful approach toward the preparation of Janus cylinders with two hemicylinders of PS and PMMA was reported by Liu et al.[17] After crosslinking the lamella−cylinder (lc) morphology of a suitable SBM block terpolymer and a sonication procedure, very long Janus cylinders with compartmentalized sides could be obtained.

From a theoretical and particularly technological point of view, the remarkable predicted surface activities of Janus structures are interesting. Binks and Fletcher[2] calculated an up to three times higher desorption energy for spherical Janus particles, as compared to particles with a homogeneous surface. In the same context, Nonomura et al.[1] recently published results of theoretical calculations about the effect of disc-shaped Janus beads on the oil/water interfacial tension. The calculations demonstrated that the adsorption energy of Janus discs can be higher by several orders of magnitude than that of ordinary classic surfactants. The promising predictions render Janus structures highly interesting as a novel class of future surfactants, which is of great scientific and industrial interest.

Here, we present for the first time the synthesis of novel disc-shaped Janus particles, composed of two different sides of polystyrene and poly(*tert*-butyl methacrylate). Using scattering and imaging techniques, we show that the particle size can be tuned, that the particles are of true Janus character, and that they form supramolecular aggregates in good solvents. Furthermore, the application of these particles to stabilize liquid−liquid interfaces will be demonstrated.

2. Results and Discussion

2.1. Synthesis and Crosslinking. The synthetic pathway to obtain disclike Janus structures is based on a template-assisted synthesis, involving crosslinking of a bulk film of a polystyrene-*block*-polybutadiene-*block*-poly(*tert*-butyl methacrylate) (SBT) block terpolymer and a subsequent sonication treatment, as outlined in Scheme 2.

For this purpose, several symmetric SBT block terpolymers were synthesized and investigated according to their microphase-separated structures. In the case of SBT, it is known that the desired so-called lamella−lamella (ll) morphology is formed over a wide range of PB fractions as long as the end blocks are of similar volume fractions.[18] The molecular characteristics of the studied SBT block terpolymers, SBT-1 and SBT-2, are summarized in Table 1. The number-average molecular weights were kept constant for the two block terpolymers, whereas the inner PB fraction was varied. It was desired to reduce the fraction of PB, based on the assumption that less sonication energy is necessary for a thin inner crosslinked layer in order to obtain soluble products after the crosslinking. The microphase separation was analyzed by transmission electron microscopy (TEM) and small-angle X-ray scattering (SAXS). Both terpolymers exhibit lamellar morphologies in the bulk state with alternating lamellae of PS and P*t*BMA, which are separated by a thin lamella of PB (see Figure 1).

Small discontinuities within the PB lamella can be seen in the case of SBT-2 due to the small fraction of PB of only 5 wt %. However, the lamella itself is still continuous, and a clear transition to a lamella−cylinder morphology or to a lamella−sphere morphology does not occur. A higher periodicity of the

(9) Erhardt, R.; Böker, A.; Zettl, H.; Kaya, H.; Pyckhout-Hintzen, W.; Krausch, G.; Abetz, V.; Müller, A. H. E. *Macromolecules* **2001**, *34* (4), 1069−1075.
(10) Xu, H.; Erhardt, R.; Abetz, V.; Müller, A. H. E.; Gödel, W. A. *Langmuir* **2001**, *17* (22), 6787−6793.
(11) Erhardt, R.; Zhang, M.; Böker, A.; Zettl, H.; Abetz, C.; Frederik, P.; Krausch, G.; Abetz, V.; Müller, A. H. E. *J. Am. Chem. Soc.* **2003**, *125* (11), 3260−3267.
(12) Sfika, V.; Tsitsilianis, C.; Kiriy, A.; Gorodyska, G.; Stamm, M. *Macromolecules* **2004**, *37* (25), 9551−9560.
(13) Kiriy, A.; Gorodyska, G.; Minko, S.; Stamm, M.; Tsitsilianis, C. *Macromolecules* **2003**, *36* (23), 8704−8711.
(14) Schrage, S.; Sigel, R.; Schlaad, H. *Macromolecules* **2003**, *36* (5), 1417−1420.
(15) Voets, I. K.; de Keizer, A.; De Waard, P.; Frederik, P. M.; Bomans, P. H. H.; Schmalz, H.; Walther, A.; King, S. M.; Leermakers, F. A. M.; Cohen Stuart, M. A. *Angew. Chem., Int. Ed.* **2006**, *45*, 6673−6676.
(16) Ishizu, K.; Satoh, J.; Toyoda, K.; Sogabe, A. *J. Mater. Sci.* **2004**, *39* (13), 4295−4300.
(17) Liu, Y.; Abetz, V.; Müller, A. H. E. *Macromolecules* **2003**, *36* (21), 7894−7898.
(18) Goldacker, T. Dissertation, University Bayreuth, Bayreuth, Germany, 1999.

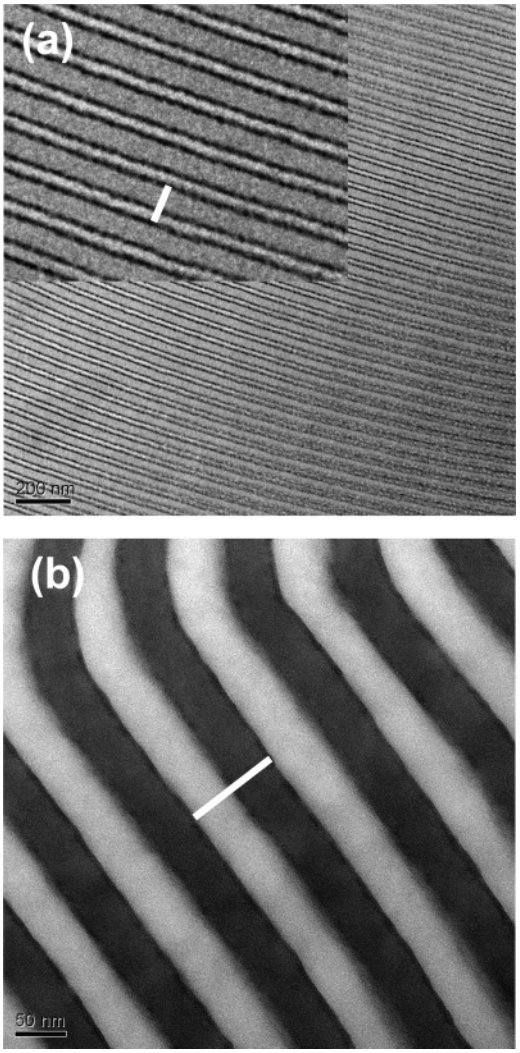

Figure 1. Transmission electron micrograph of an ultrathin section of SBT-1 (a) and SBT-2 (b) films after staining with OsO_4. The ultrathin film was imaged using standard (a) and carbon coated (b) TEM grids. The white bar indicates the long period of the periodicity of the structure.

Table 1. Molecular Characterization of the SBT Block Terpolymers

	composition[a]	block DP[b]	$10^3 \times M_{n,\,MALS}$ (M_w/M_n)	$R_{g,z}$ [nm] (STD)[c]
SBT-1	$S_{42}B_{10}T_{48}$	$S_{536}B_{246}T_{449}$	133 (1.06)	18.6 (9%)
SBT-2	$S_{45}B_5T_{50}$	$S_{575}B_{123}T_{468}$	133 (1.03)	18.6 (13%)

[a] Indices correspond to the weight fractions (in %), as calculated from the ^{1}H NMR spectra (S = polystyrene, B = polybutadiene, T = *tert*-butyl methacrylate). [b]Number-average degree of polymerization of each block. [c]*z*-Average root-mean-square radius of gyration as determined by GPC-MALS measurements (STD = standard deviation).

perforations cannot be observed, and thus the morphology is best described as an irregularly perforated lamella−lamella structure. A clear breakup of the PB layer was observed in the case of a symmetric SBT block terpolymer having a fraction of only 4 wt % of PB (not shown here). The microphase-separated structure of SBT-1 can unambiguously be assigned to a lamella−lamella (ll) morphology. Since it is known that TEM micrographs may not always reflect the true dimensions of the long periods of the structures due to electron-induced degradation and shrinkage of methacrylate blocks, SAXS measurements were performed (Figure 2).[19]

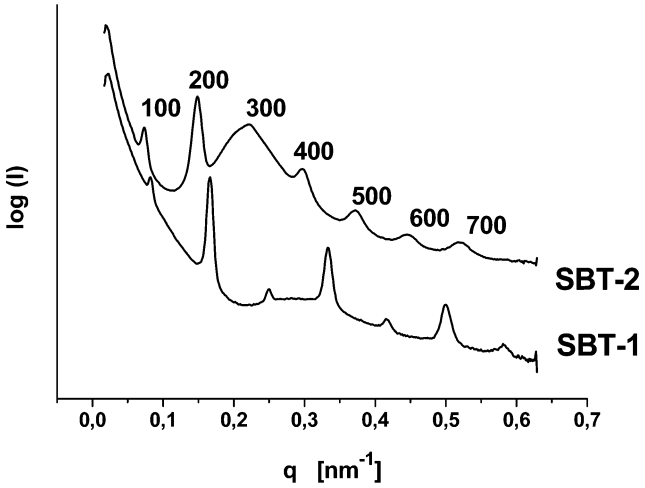

Figure 2. SAXS diagrams after azimuthal integration of the intensity as a function of the scattering vector *q* for SBT-2 and SBT-1. The SAXS pattern of SBT-2 was multiplied by 15 to allow a better separation.

Both SAXS patterns exhibit the characteristic peak distributions for lamellar block copolymer structures, meaning the reflections are integer multiples of the first-order peak q^* ([100]). The positions of the reflections allow the calculation of the long period, d, of the structures via $d = 2\pi/q^*$. The deduced values are $d = 80$ nm and $d = 86$ nm for SBT-1 and SBT-2, corresponding to the ones which were determined by TEM investigations (SBT-1: d = 78 nm; SBT-2: $d = 86$ nm), when carbon coated grids were used for the imaging process.

In conclusion, both SBT block terpolymers exhibit the desired lamella−lamella morphology which is necessary for the preparation of the flat Janus particles.

The crosslinking of the inner polybutadiene layer preserves the preorientation of the two outer non-centrosymmetric sides, PS and P*t*BMA. The desired Janus particles can be obtained after dissolution of the crosslinked block terpolymer templates by means of sonication. On basis of the determined long periods it is possible to estimate the sheet or disc thickness to be around 35−45 nm, resembling a polymer brushlike flat particle.

Two strategies were employed for the crosslinking of the SBT block terpolymer templates. Both "cold vulcanization" by S_2Cl_2 and radical crosslinking using AIBN—and its optimization by the thiol−polyene procedure[20−24]—have proven to be effective routes for crosslinking polybutadiene microdomains. The success of the crosslinking strategies was confirmed by TEM, which showed the clear persistence of the lamellar morphologies after crosslinking (see Figure S-1, Supporting Information for further details).

2.2. Sonication and Solution Properties. 2.2.1. Dynamic Light Scattering. After successful crosslinking of the block terpolymer templates with either of the methods mentioned above, the corresponding insoluble fractions were subjected to a sonication procedure in order to obtain soluble Janus discs.

(19) Breiner, U.; Krappe, U.; Thomas, E. L.; Stadler, R. *Macromolecules* **1998**, *31* (1), 135−141.
(20) Jacobine, A. F. *Radiation Curing in Polymer Science and Technology*; Elsevier Applied Science: London, 1993; Vol. 3, p 219.
(21) Decker, C. *Prog. Polym. Sci.* **1996**, *21* (4), 593−650.
(22) Decker, C.; Nguyen Thi Viet, T. *Macromol. Chem. Phys.* **1999**, *200* (8), 1965−1974.
(23) Decker, C.; Nguyen Thi Viet, T. *Macromol. Chem. Phys.* **1999**, *200* (2), 358−367.
(24) Decker, C.; Nguyen Thi Viet, T.; Hien Le, X. *Macromol. Symp.* **1996**, *102*, 63−71.

Thus, the solutions of swollen crosslinked gels were treated with high-energy ultrasound in a temperature-controlled cell until a semitransparent solution was reached. The effective crosslinking and the persistence of the chemical composition were verified after crosslinking and sonication to coincide with the postulated mechanism of the template-assisted synthesis toward Janus discs (see Supporting Information Figure S-2 for ^{1}H NMR characterization).

After this procedure, dynamic light scattering measurements were conducted in order to investigate the sizes of the resulting flat Janus particles and their distribution. Since the appearance of polydisperse and also multimodal distributions was expected using sonication for homogenizing the solutions, the analysis of the normalized field autocorrelation function, $g_1(t)$, was mainly restricted to the use of the CONTIN algorithm. The use of the classical cumulant anaylsis,[25] which has the benefit of enabling an estimation of the sample polydispersity via the second cumulant, μ_2, is limited within this work. In the case of multimodal samples or moderately to highly polydisperse samples, the series expansion of the cumulant analysis shows only a slow or no convergence at all,[26] leading to erroneous results. It may only be applied for samples whose CONTIN analysis had previously shown a unimodal and relatively narrow distribution.

The investigation of angular dependent scattering data can be used to draw conclusions about the actual shape of particles in solution, in static as well as in dynamic light scattering. An angular dependence may have several origins: large flexible molecules, anisotropic shapes, and polydispersity. For large anisotropic molecules, like rods and disc-shaped molecules, flexion, bending, and rotational diffusion occur in addition to the standard translational diffusion. Their contributions to the scattered light are dependent on the wave vector, q, thus inducing an angular dependence. Neither much theoretical nor much experimental work has been reported in the case of disclike scatterers, which is mainly due to the limited access to free disclike molecules. A formulation of the dynamic form factor for the intensity of scattered light from thin discs was proposed by Fujime and Kubota and applied to the study of membrane fragments.[27−29] The theoretical expression for the average decay rate for a disclike scatterer with radius R is given by eq 1.[28]

$$\frac{\Gamma}{q^2} = D + \left(\frac{R^2}{4}\right)\Theta g_1(qR) + (D' - D'')\left[g_2(qR) - \frac{1}{3}\right] \quad (1)$$

$$\lim_{q\to 0}\frac{\Gamma}{q^2} = D \quad (2)$$

D, D', D'', and Θ are the average translational diffusion coefficient, the diffusion coefficients perpendicular and parallel to the disc plane, and the average rotational diffusion coefficient of the disc, respectively. $g_1(qR)$ and $g_2(qR)$ are functions, which can be calculated numerically and depend only on qR. The calculated values can be found elsewhere;[28] in the limit of $qR = 0$, we find $g_1(qR) = 0$ and $g_2(qR) = {}^1/_3$, so that Γ/q^2 provides the average translational diffusion coefficient upon extrapolation to $q = 0$ (eq 2). At larger qR, meaning also larger q^2, additional modes are present.

Figure 3 displays the normalized field autocorrelation functions and their CONTIN plots as well as the angular dependent scattering data for various samples of Janus discs after different sonication times.

A shift of the characteristic decay time of the normalized field autocorrelation functions can be observed for the different angles, which translates into different, average decay rates, Γ, diffusion coefficients, or apparent hydrodynamic radii in the corresponding CONTIN plots.

All curves presented in Figure 3c are typical of what one expects for disclike structures, meaning a curved increase of Γ/q^2 with the squared scattering vector, q^2. This decrease is expected to level off slightly at higher q-values, depending of course on the values of qR. It is worth noting that Kubota et al.[27,29] and van der Kooij et al.[30] found that the polydispersity affects mainly the curvature of the plot of the angular dependent diffusion coefficients of flexible and nonflexible disclike scatterers, respectively. In conclusion, the obtained scattering data strongly indicates the presence of disclike scatterers in solution, whose translational diffusion coefficients and apparent hydrodynamic radii can be calculated after extrapolating to zero angle.

In order to further elucidate the size evolution in dependence of the crosslinking method and the sonication energy and duration, DLS measurements at different stages of the sonication and at different sonication energies were performed. Figure 4 displays the dependence of the apparent hydrodynamic radius, $\langle R_h\rangle_z$, on the sonication duration and the amplitude.

Generally, a characteristic decay of the hydrodynamic radii can be observed with increasing sonication time for all homogenization procedures. The curves follow an exponential decay, indicating that in the beginning of the ultrasound treatment the large particles are fragmented into significantly smaller ones, causing the rapid decrease. After a certain time (20−30 min for SBT-1, 5−10 min for SBT-2) the curves show a more asymptotical behavior. At this stage the particle size decays much more slowly. Consequently, there is some higher resistance to the introduced sonication energy. This resistance is presumably due to the higher mobility of the smaller structures and an accompanying higher resistance and more flexible adaptation to the shock waves produced by the ultrasound. An increase in the sonication amplitude from 10% to 70% leads to a much faster disruption of the particles, and the plateau is reached earlier. The plateau values are similar for all three sonication amplitudes; however, the lowest one is attained with the highest sonication amplitude.

The fits presented in Figure 4 were performed using a combination of two exponential functions. The ratio of the two decay constants is about 14. Hence one may conclude a kind of two-step mechanism for the particle disruption. The results demonstrate convincingly the facile tunability of the size of the Janus discs. The particle sizes can be adjusted from the micrometer range down to the nanometer level, thus covering a large mesoscopic length scale.

(25) Koppel, D. E. *J. Chem. Phys.* **1972**, *57* (11), 4814−4820.
(26) Brown, J. C.; Pusey, P. N. *J. Chem. Phys.* **1975**, *62* (3), 1136−1144.
(27) Marque, J.; Ikegami, A.; Kubota, K.; Tominaga, Y.; Fujime, S. *Biophys. J.* **1986**, *50* (1), 139−144.
(28) Fujime, S.; Kubota, K. *Biophys. Chem.* **1985**, *23* (1−2), 1−13.
(29) Kubota, K.; Tominaga, Y.; Fujime, S.; Otomo, J.; Ikegami, A. *Biophys. Chem.* **1985**, *23* (1−2), 15−29.
(30) van der Kooij, F. M.; Philipse, A. P.; Dhont, J. K. G. *Langmuir* **2000**, *16* (12), 5317−5323.

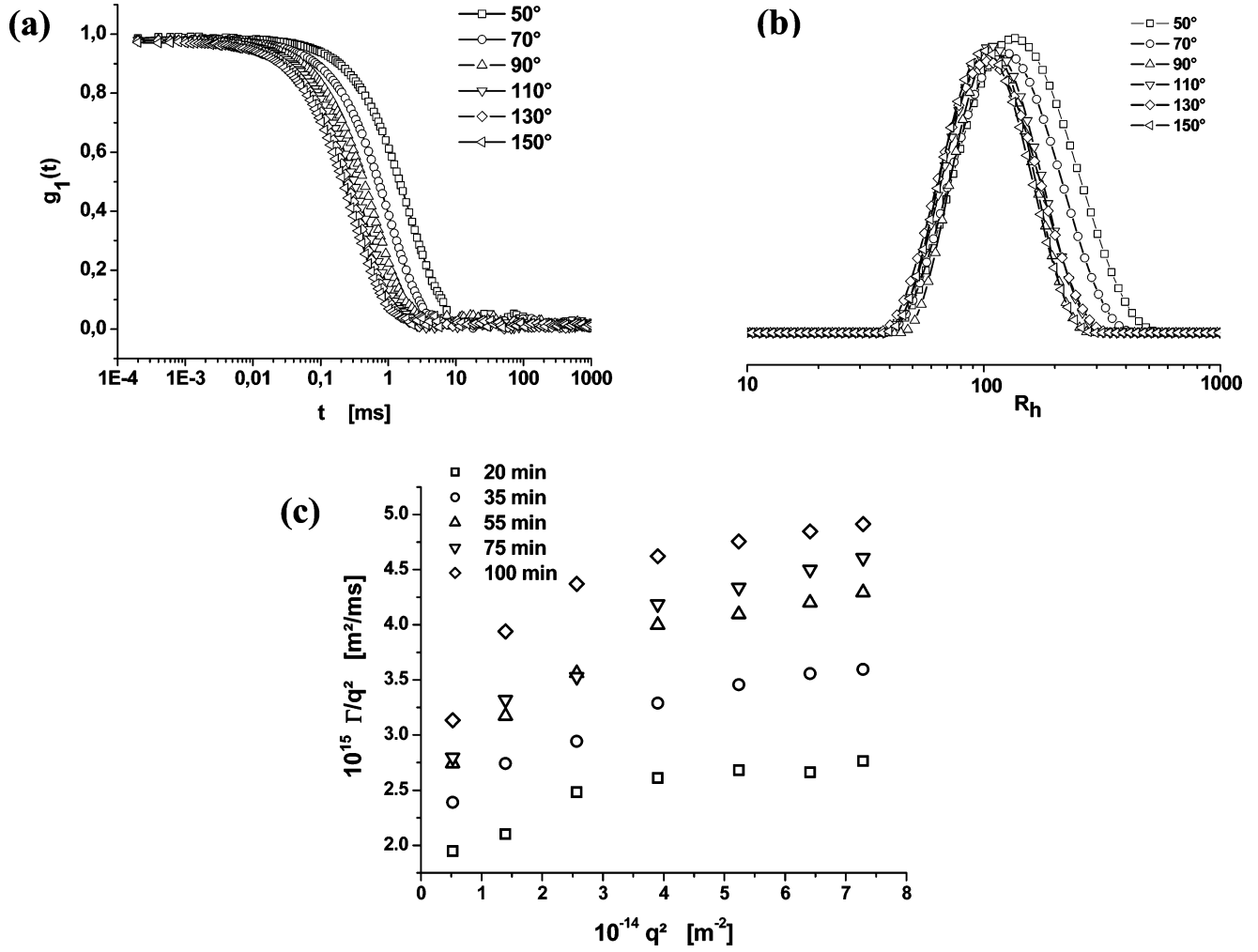

Figure 3. Normalized field autocorrelation functions (a) and their corresponding CONTIN plots (b) for different angles (SBT-1; 5 wt % AIBN in presence of 5 wt % TRIS, 55 min sonication at 10% amplitude, measured in THF). (c) Dependence of Γ/q^2 on the squared scattering vector, q^2, for various sonication times.

A more detailed look at the different curves reveals further peculiarities between the two different block terpolymer templates. One of the characteristic differences for the sonication of the templates, SBT-1 and SBT-2, is the fact that the former requires longer durations and thus more energy for reaching a solution, which does not show any visible sedimentation. For instance, 300 and 30 s are necessary to obtain homogeneous solutions at a sonication amplitude of 30% for SBT-1 and SBT-2 templates, respectively. Since the extents of crosslinking are similar for the radical crosslinking of the two block terpolymer templates, this difference is related to the different fractions of crosslinkable polybutadiene in the two block terpolymers. Second, the initial hydrodynamic radii after reaching the solution state for the two kinds of crosslinked block terpolymers are remarkably different, as can be seen from the values for the hydrodynamic radii at short sonication times (0−10 min). The hydrodynamic radii for the SBT-2 based Janus particles ($\langle R_h \rangle_z = 140-200$ nm) are smaller by a factor of 2 to 3 than the sizes obtained for the crosslinked and sonicated SBT-1 block terpolymers ($\langle R_h \rangle_z = 330-470$ nm). This can be explained considering the very thin, partially discontinuous, and not fully crosslinked polybutadiene layer of the SBT-2 block terpolymer. Hence, this template needs much less energy and breaks more frequently, leading to the observation of smaller disc sizes after short sonication times. Values for the hydrodynamic radius much larger than 200 nm cannot be reached using SBT-2. The crosslinked material starts to become soluble at sonication times around 30 s, where the *z*-average hydrodynamic radius is around 140−200 nm, depending on the crosslinking method. A minimum sonication duration of 30 s is yet required in order to solubilize some bigger particles. In addition, the influence of the crosslinking agent, AIBN or S_2Cl_2, can be compared in Figure 4b. The cold vulcanization leads to the observation of larger particles at all stages of the ultrasound homogenization. This is presumably due to a larger extent of the crosslinking in the case of the cold vulcanization and reflects also the morphological changes upon swelling the SBT-2 template in isooctane. TEM investigations had shown a transformation of the perforated into a continuous lamella upon addition of isooctane. Therefore, a more continuous crosslinking can take place during the cold vulcanization.

A further difference between the two block terpolymer templates can be observed with respect to the plateau value. Whereas the hydrodynamic radius for the SBT-1 based flat Janus particle is in the region 110−150 nm, it is only half of it for the SBT-2 based particles. This demonstrates that not only the size of the molecules is important to withstand the mechanical forces of the sonication procedure but also the thickness of the

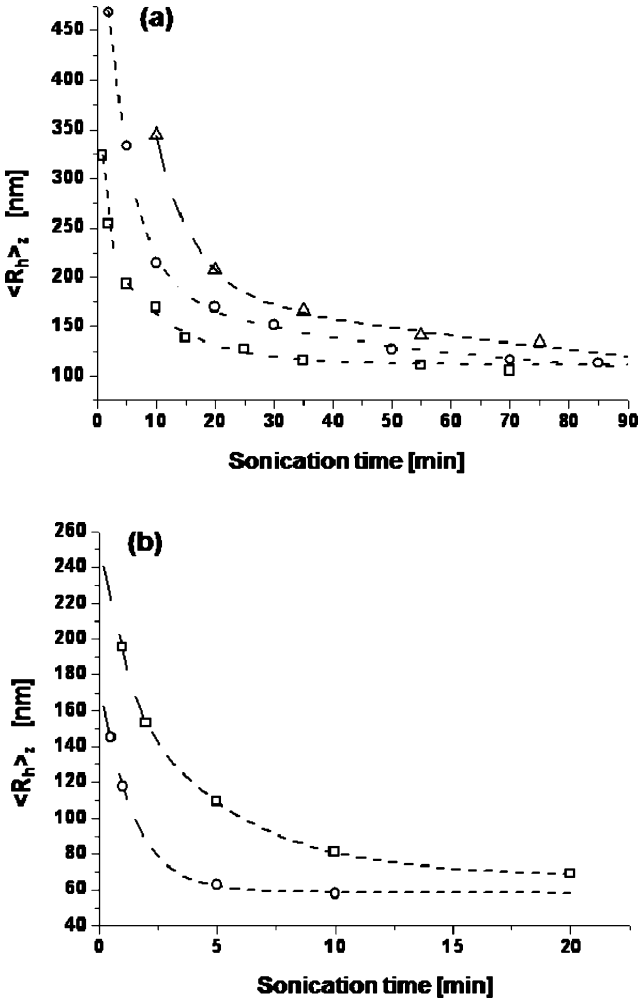

Figure 4. Dependence of $\langle R_h \rangle_z$, obtained after extrapolating the angular dependent data to $q^2 \rightarrow 0$, on the sonication power and duration for differently crosslinked block terpolymer templates. Traces for SBT-1 (a) crosslinked with the thiol−polyene process (5 wt % AIBN in presence of 5 wt % TRIS) are shown for different sonication amplitudes ((□) 70%, (○) 30%, (△) 10%). (b) Size evolution for the sonication (30% amplitude) of SBT-2 block terpolymers which were cold vulcanized with sulfur monochloride ((□) 1.5 vol % S_2Cl_2) or crosslinked with the thiol-polyene process (○).

inner crosslinked layer plays a role. If one assumes a kind of bending modulus for both kinds of disclike Janus particles, it is obvious that the SBT-1 based particles should have a higher one as the higher content of polybutadiene leads to a tighter network layer within those. Consequently, the mechanical strength and the resistance toward ultrasound are better, explaining the higher value for the plateau.

2.2.2. Mechanism of Particle Disruption. Figure 5 shows the time-dependent evolution of the normalized field autocorrelation functions and the size distribution for a representative sample of Janus discs (SBT-1, 5 wt % AIBN, 5 wt % TRIS, 30% amplitude) during the sonication.

The correlation functions show a distinct shift of the characteristic decay time, τ, toward lower values, with increasing duration of the sonication, which correlates with an overall decrease in particle size. The CONTIN plots on the right-hand side of Figure 5 show bimodal distributions for short sonication times (t < 20 min) with peaks at around 150 nm and 600−1000 nm.

It can be seen that the latter peak diminishes during the sonication and vanishes totally for sonication times longer than 20 min. Continuing the sonication for longer than 20 min leads then to a gradual shift of the monomodal peak maximum at $\langle R_h \rangle_z = 80-120$ nm, which can also be seen in the asymptotical behavior in Figure 4. The particles are no longer disrupted, but only very small fragments are cut off. Indeed, for very long sonication times (140 min) a peak for very small fragments can appear. A complete disruption of the particles seems to be only possible for particles above a critical threshold value (here around $\langle R_h \rangle_z = 500$). The loss of small fragments of the discs does certainly already occur during the early stages of the sonication, but it is invisible as the rapid decrease due to the disruption of large particles dominates the size distribution curves.

This observation is consistent with the above-mentioned mechanism, that in the beginning of the sonication the large particles are disrupted very quickly into significantly smaller ones; i.e., they are divided into small parts. A splitting off of small splinters can clearly not account for the rapid decay and the observation of a bimodal distribution of this kind. Instead of the evolution of the size distribution determined here, a gradual shift of the peak should occur and a peak corresponding to very small fragments should arise earlier.

Another phenomenon can be observed during continuing sonication in the plateau region. It can be seen that the size distribution of the Janus discs narrows progressively. Since unimodal distributions can be obtained for longer sonication times, the cumulant analysis can be performed in order to obtain values for the polydispersity indices of the structures. The calculated polydispersities are in the range 1.3−1.1 for sonication times between 20 and 85 min. Consequently, the size distribution is narrowed significantly, and Janus discs with moderate size distributions can be obtained by continued sonication.

2.3. Visualization. Several imaging techniques were used in order to visualize the resulting disclike Janus structures. The focus of these investigations was to address the issues, whether the particles aggregate and how the actual shape looks like. In particular one might expect a back-to-back stacking of the particles, i.e., an aggregation of two particles into dimeric superstructures. Furthermore, it is interesting to know whether the particles possess a more sheetlike character with irregular edges or if they can reach a disclike appearance.

In general, the particles show a very strong tendency to adsorb onto standard silicon and mica substrates. It was found that the particles tend to aggregate strongly while depositing on the surface. One driving force to create these assemblies is certainly the tendency to minimize energetically unfavorable edges of the flat Janus particles. A good separation can only be obtained when depositing the sample from an ultradilute solution.

2.3.1. Scanning Electron Microscopy. Figure 6 shows an SEM image of flat Janus particles deposited onto a silicon wafer from a very dilute (0.1 mg/L) $CHCl_3$ solution.

Various discs tend to coalesce and form a continuous film as can be seen on the left-hand side of the image. On the contrary, molecularly dispersed and well-separated particles can be seen on the right-hand side. The size distribution of these nonaggregated particles resembles those in the solution as determined by DLS of this sample. The particles themselves

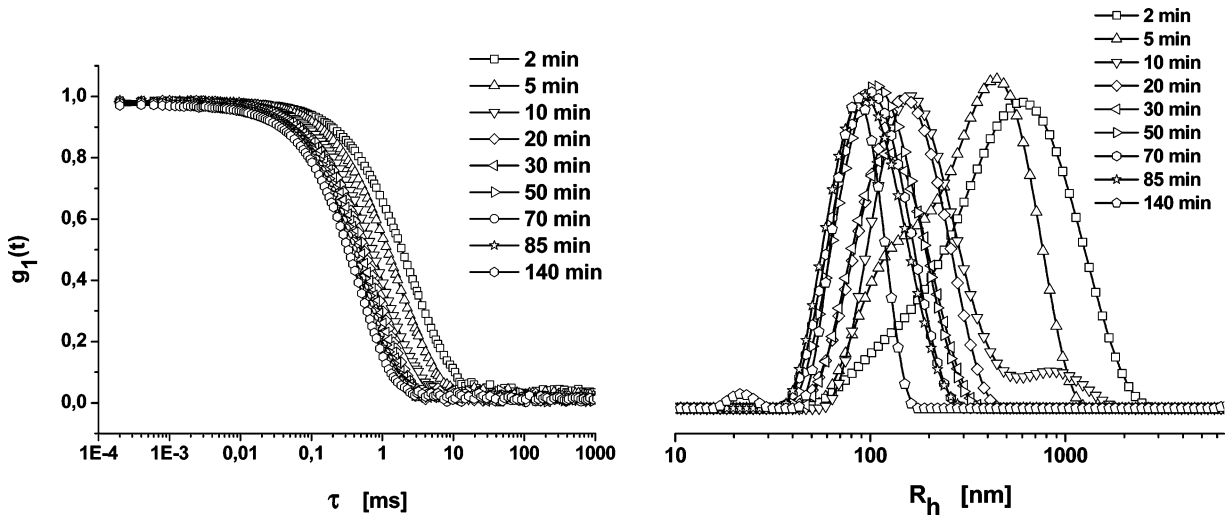

Figure 5. Normalized field auto-correlation functions (left) at 90° for a Janus disc sample (SBT-1, 5 wt % AIBN, 5 wt % TRIS) which was sonicated at 30% amplitude. Corresponding size distributions after evaluation with the CONTIN algorithm (right).

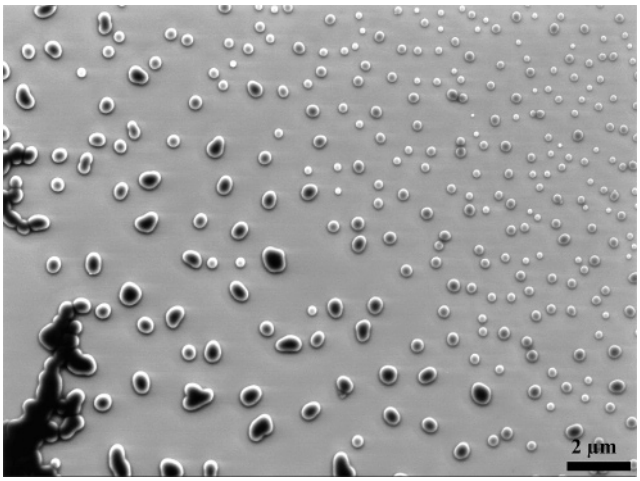

Figure 6. SEM images obtained from a dip-coated sample of Janus discs (c = 0.1 mg/L in $CHCl_3$; SBT-1, 5 wt % AIBN, 5 wt % TRIS, sonication at 30% amplitude) on silicon (3 kV acceleration voltage).

exhibit a surprisingly circular to ellipsoidal shape. On account of this observation, more attention was drawn on the shape development of the particles on substrates, as well as in solution. In order to gain further information about the particles, especially with respect to their heights and detailed shapes, a thorough scanning force microscopy (SFM) investigation was performed. SFM can further improve the resolution of the Janus particles and resolve more structural details than SEM.

2.3.2. Scanning Force Microscopy. Several representative SFM images of disclike Janus structures obtained by crosslinking of the SBT templates via the cold vulcanization or the free radical crosslinking process will be discussed in the following. To the best of our knowledge, this is the first detailed investigation of semiflexible flat polymeric nanoobjects adsorbed onto surfaces by means of scanning force microscopy.

The images in Figure 7 reveal a multitude of interesting features. First of all, the discs are round in most of the images as similarly observed by SEM. The inset in Figure 7b shows the aggregation of two small and more asymmetric particles, confirming the presence of asymmetric objects and the possibility to image those under the applied measurement conditions. The development of round-shaped particles is presumably caused by subjecting the crosslinked material to ultrasound energy. The particles will preferentially break at existing cracks, and protrusions standing out of the main particle will be cut off most easily. These processes lead to a rounding off and "shaving" of the particles. As a consequence the particles will develop a round, more disclike appearance, as can be seen in most of the images.

Really anisometric sheetlike structures can only be found in the very beginning of the sonication procedure for the Janus particles based on the SBT-1 template (see Figure 8 and Supporting Information for cryo-TEM images of the early state of sonication). Some potential breaking points are highlighted with arrows in Figure 8. Breaking the particles at the highlighted crack lines will result in two significantly more spherical particles, in particular for the particle shown on the left-hand side of Figure 8. This observation strongly supports the aforementioned influence of the sonication treatment and explains the absence of large protrusions and deformed noncircular objects.

Second, the phase image in Figure 7b shows an interesting core−corona contrast for the particles, indicating that the elasticity of the top of the particles is somewhat different from that of the corona. The corona probably consists of spread chains of the underlying side of the Janus disc. Therefore a different material is probed at the outer area of the structure. If there was no coronal segregation, this kind of core−corona structure in the phase contrast would not be expected, as a mixed corona should not give any phase contrast. Due to the polar nature of the substrate and the higher polarity of the P*t*BMA as compared to PS, P*t*BMA is adsorbed to the substrate.

During the thorough analysis of the height profiles of the particles, it was found that many structures show a droplet-shaped section profile. Additionally, a size dependence of the height on the overall particle size could be found. These effects are presumably caused by the rapid drying and the kinetic entrapment of the dropletlike shape which develops during drying for each individual Janus disc (see Supporting Information for images and further explanation). In order to explore this phenomenon and to prove whether the structures can be kinetically frozen, substrates with formerly deposited Janus discs were either heated to 150 °C in vacuo or annealed in toluene

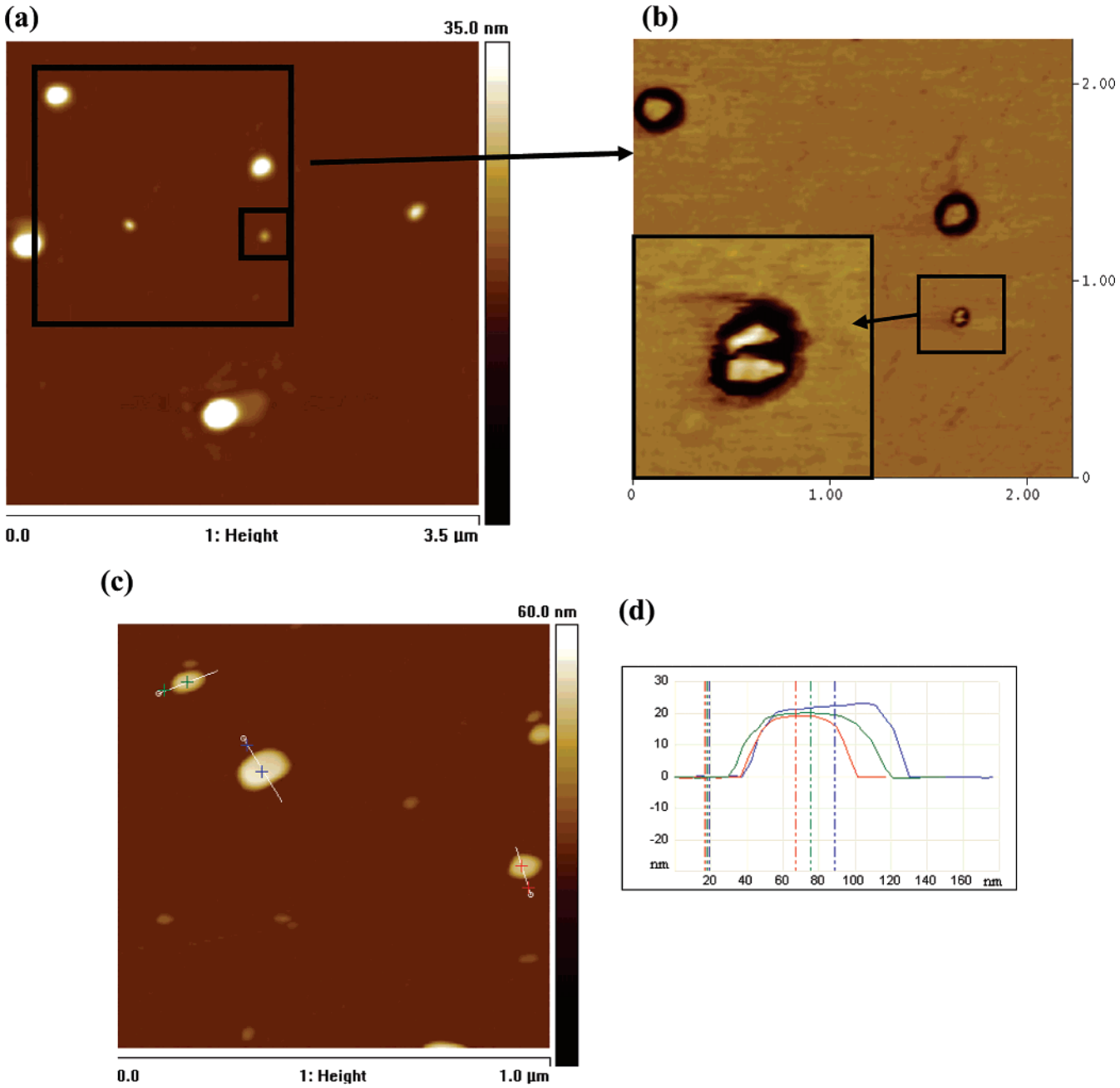

Figure 7. (a and c) SFM height image obtained from a sample of Janus discs (SBT-2, S_2Cl_2, sonication for 20 min at 30% amplitude). (b) Phase image of a part of image (a), containing a further magnified inset. (d) Section analyses corresponding to the lines in image (c). All samples were dip-coated from a $CHCl_3$ solution (c = 0.1 mg/L) onto silicon wafers.

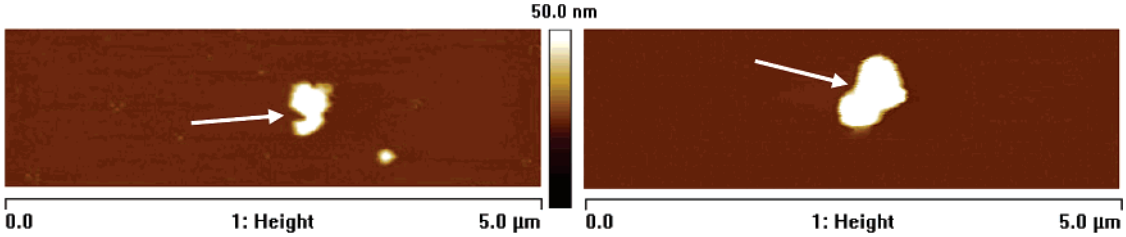

Figure 8. SFM height images obtained from a sample of Janus sheets (SBT-1, 5 wt % AIBN, 5 wt % TRIS, sonication for 3 min at 30% amplitude) dip-coated from a $CHCl_3$ solution (c = 0.1 mg/L) onto mica. The white arrows highlight potential breaking points of the structures.

vapor (90 °C) in order to allow a thermal relaxation of the particles. Both methods should provide enough energy to allow a segmental movement and a reorientation of the structures. Figure 9 shows two representative high-resolution SFM images obtained from such annealing experiments. The images show that several changes developed after the two annealing procedures. The plateau is now very pronounced, in contrast to nonannealed structures, and the height approaches similar values

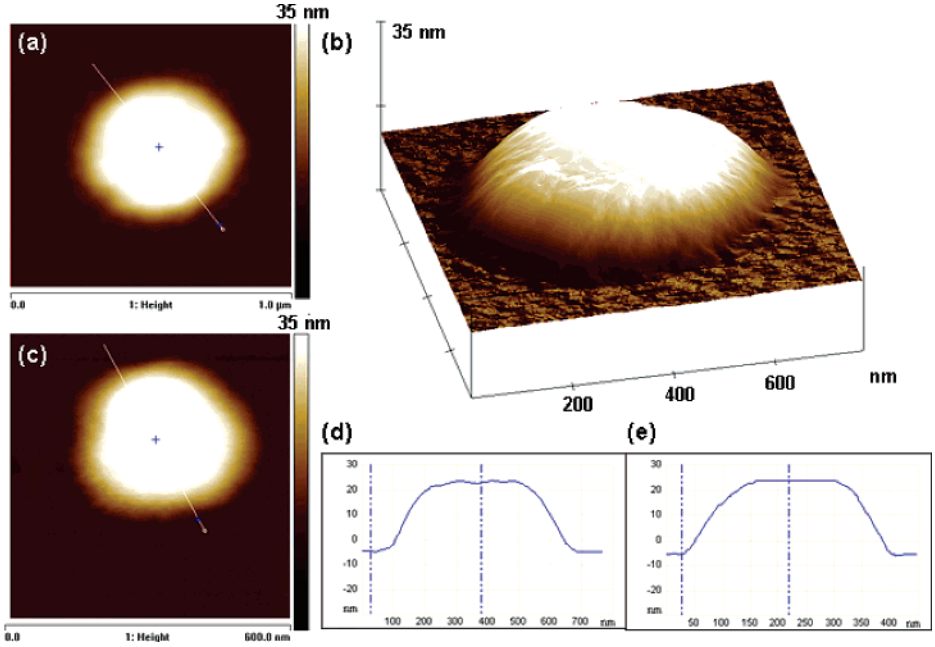

Figure 9. SFM height image obtained from a sample of Janus discs (SBT-2, 5 wt % AIBN, sonication for 1 min at 30% amplitude) using an ultrasharp tip (R_{Apex} < 2 nm) for imaging. The sample was dip-coated from a 0.1 mg/L $CHCl_3$ solution onto mica and annealed at 150 °C in vacuo (a) or at 90 °C in toluene vapor (c). (b) 3D surface plot of (a). (d and e) Section analyses corresponding to the lines shown in the height images (a and c, respectively).

of ca. 28−35 nm for all particles, which are very reasonable values for the disc thickness. Based on the TEM investigations of the uncrosslinked block terpolymer films, values for the disc thickness between 30 and 40 nm are expected. The dropletlike shape changes to a significantly flatter one, which is expected for the brushlike disc-shaped object. The plateau itself is totally flat over 150−300 nm as can be seen in the two section analyses and the 3D surface plot. Therefore, the kinetically trapped droplet-mimicking structure, induced during the solvent evaporation, is brought much closer to the thermodynamic equilibrium.

One point, which does not dramatically change upon annealing, is the smooth height increase at the border of the Janus discs. Typically, this onset remains in the region 60−120 nm. However, considering the proportions of the polymer chains (e.g., contour length of P*t*BMA, $l_c \approx 115$ nm) and the strong tendency of the particles to adsorb onto the interfaces (see above), the observed dimensions of the height increase can be understood (see inset in Scheme S-1). It appears that the contributions of the interfacial energy of the system are dominant at the outer regions of the particle, whereas the brushlike behavior dominates the structure in the centers of the particles. Based on the considerations of the energetic contributions to the system, the appearance of the flat Janus particles on surfaces can now be reasonably understood.

2.3.3. Cryogenic Transmission Electron Microscopy (Cryo-TEM). Cryo-TEM was chosen in order to explore the particle shape *in situ* in solution and to investigate the samples toward the self-assembly into superstructures in a concentrated solution. The investigation of particles deposited from solution in the semidilute and concentrated regime by SFM or SEM is not possible due to the strong adsorption and aggregation tendency of the particles. Hence it would not be clear whether true aggregates were imaged or whether the assemblies were artificially constructed during the deposition process. Therefore, cryo-TEM investigations in a slightly selective good organic solvent, THF, were performed for a variety of different samples in the more concentrated regime, typically with concentrations higher than 1 mg/mL. Figure 10 shows a representative overview of images with aggregated Janus discs (more images can be found in the Supporting Information).

Despite the low contrast (mass density × specimen thickness) between material and solvent, a layered structure can clearly be seen in the image. Several arrows highlight parts for which distinct layers can be seen most easily. Moreover, the cryo-TEMs convincingly demonstrate the absence of vesicular structures, which could not be ruled out in the beginning of the investigation of flat Janus particles.

In order to further elucidate the layered structures, a cross-sectional analysis is shown in Figure 10d. The cross section is based on the gray scale originating from the contrast variations within the sample. Two distinct layers can be seen, and additionally, the particles show a very flat profile in the center. This suggests that the particles are indeed flat and that the superstructures are composed of two back-to-back stacked Janus discs. Furthermore, it can be seen that the particles are actually circular and that the above-mentioned mechanism of ultrasound-induced rounding of the particles holds. The aggregation process into superstructures is somewhat surprising as THF is a good solvent for both sides, PS and P*t*BMA. Due to the very good solubility of P*t*BMA in a variety of solvents, we expect that PS forms the inner solvent-swollen part of the assemblies. The driving force for the self-assembly process cannot be readily understood and deserves further investigations in the future.

A similar unexpected aggregation into superstructures was demonstrated for the spherical Janus micelles. Therefore, this self-assembly behavior can be attributed to the unique Janus character of the disclike particles. In the case investigated here, a time-dependent aggregation process is indicated by the cryo-TEM investigations. For instance, if a sample is analyzed directly after applying high shear stress via passing a 1 μm PTFE filter, mainly molecularly dispersed Janus discs can be observed. In contrast, if the sample is allowed to undergo an aging process

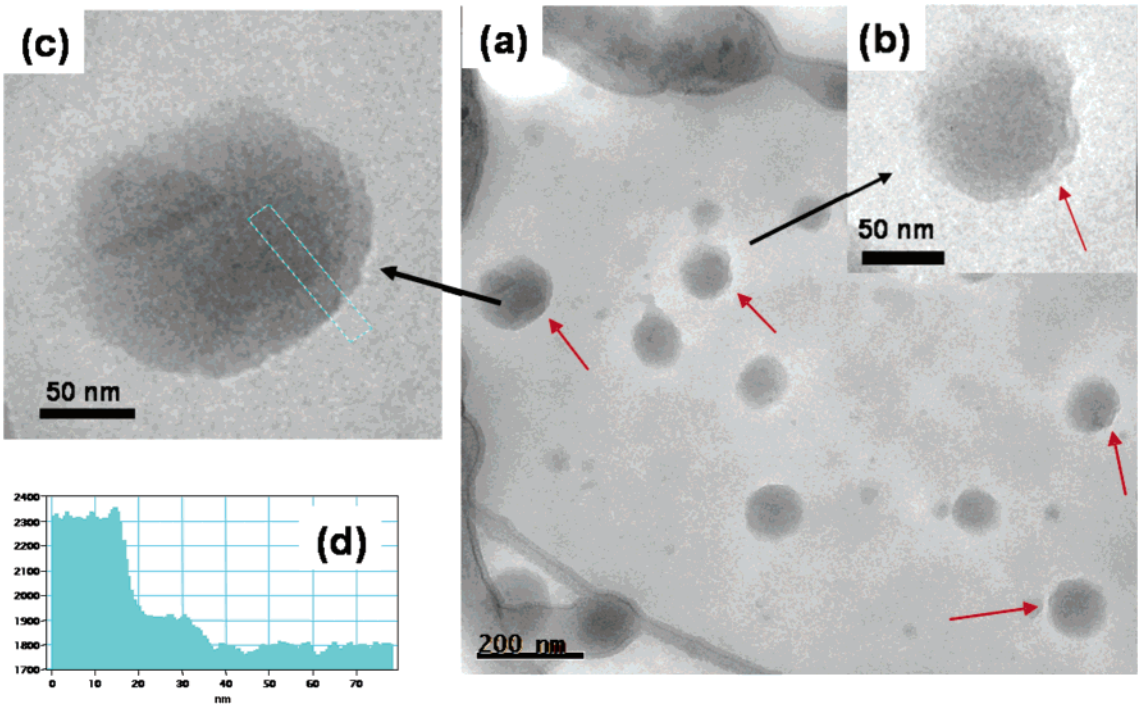

Figure 10. Cryogenic transmission electron microscopy images of a sample of Janus discs in tetrahydrofuran. The sample was allowed to equilibrate for several weeks at room temperature before imaging. (a) Overview with two magnified images (b and c). The red arrows highlight areas in which layered structures can be observed most easily. (d) Cross-section analysis of the bar shown in image (c), demonstrating the layered structure and the flat structure inside of the aggregate.

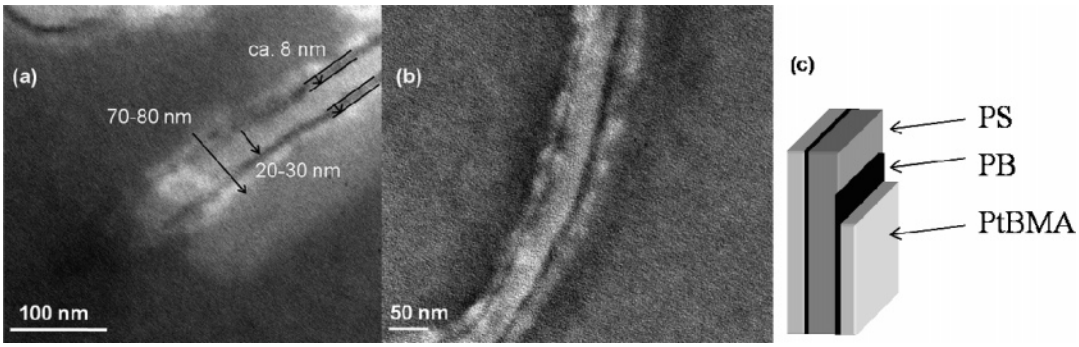

Figure 11. TEM images of embedded Janus particles (based on the SBT-1 template) after microtome cutting and staining with OsO_4. The particles were embedded from a concentrated solution of THF (a) or acetone (b) in the presence of photo-crosslinkable silicon oil. Image (c) depicts a schematic representation of the different layers.

(several days), the fraction of aggregates increases significantly. Unfortunately, it is not straightforward to follow this time-dependent process, e.g., by means of DLS or fluorescence correlation spectroscopy, as back-to-back stacking has only a very small influence on the diffusion coefficient. This difference can hardly be measured for a polydisperse system.

In conclusion, the cryo-TEM investigations show convincingly that the particles exist as disclike structures in solution. Moreover, the Janus discs tend to self-assemble reversibly into loose solvent swollen superstructures in moderately concentrated solutions. The structure of those aggregates can be described by back-to-back stacking of the Janus discs.

2.3.4. TEM Analysis of Embedded Janus Discs. TEM of embedded Janus discs was done in order to confirm the inherent multicompartment structure and the aggregation of Janus discs into superstructures. The subsequent images were obtained after rapid drying of THF or acetone solutions containing flat Janus particles and a crosslinkable silicon oil. After crosslinking, microtome cutting was performed and the ultrathin sections were stained with OsO_4 vapor prior to TEM imaging (see Figure 11).

Long cylindrical structures can be found within the ultrathin sections. Long cylinders can only originate from embedded flat structures, thus confirming the presence of Janus discs in the solution. A close look at the cross section of the structures reveals the presence of several layers. The structure found corresponds to a back-to-back stacked assembly of the Janus discs with the polystyrene part in the center. This structure can be found independently of the solvent used. Note that acetone is a nonsolvent for polystyrene and thus forces aggregation of the Janus discs into a layered assembly. Since exactly the same structure can be found in the case of THF as solvent for the Janus discs, an aggregation of the Janus discs in the THF solution appears most likely. The grayscales found for the different layers originate from the elemental composition of the different parts. The thin crosslinked butadiene layer, whose residual double bonds were stained with OsO_4, appears very

dark. In contrast, the inner polystyrene layer appears much brighter as almost no OsO_4 is present there. The overall surrounding silicon oil appears slightly darker than the PS part due to the large content of silicon. The P*t*BMA part at the outside is again bright, due to the decomposition of the P*t*BMA in the electron beam. Thus an average contrast originating from degraded P*t*BMA and surrounding silicon oil can be found.

The length scales, as indicated in image (a), correspond closely to what was found from the initial SBT-1 template. Note that the height of the nonaggregated Janus discs was found to be around 30−35 nm as imaged by SFM. Thus this value corresponds to half of the thickness found for the back-to-back stacked assembly here. In the experiments it was not possible to image single nonaggregated Janus dics, which is due to the fact that the concentration of the solution is high, typically in the range 10−30 mg/mL. Moreover, during the evaporation of the solvent, the concentration increases dramatically above a critical aggregation concentration. Nonaggregated Janus discs can only be imaged by SFM and SEM at very high dilution.

Besides, image (a) shows the ends of two assembled structures (center and upper right corner). It can be seen that the assemblies are open at the end and that the polybutadiene layer does not surround and cover the complete inner PS part.

In conclusion, the embedding experiments ultimately confirm a flat multicompartment type architecture and give a strong indication for a self-assembly of the Janus disc in THF.

2.4. Behavior at Liquid−Liquid Interfaces. As already mentioned in the introduction, calculations show that Janus discs should have a much stronger adsorption energy at liquid−liquid interfaces than ordinary low-molecular weight surfactants of similar composition[1] and most likely than homogeneous particles of similar size. The herein synthesized Janus discs are ideally suited for investigating this phenomenon experimentally. The predictions for spherical Janus particles were recently verified by Glaser et al.[31] A remarkable decrease of the oil/water interfacial tension was found upon introduction of Janus character into the surface active particles. Janus structures may thus be of great importance as future surfactants.

One way of determining the influence of particles at liquid−liquid interfaces is to analyze the interfacial tension isotherms of a solution of the desired material, e.g., via the pendent drop method. Recording and analyzing the droplet shape of two immiscible liquids, one containing the dissolved material, via a digital camera system, provide the time-dependent evolution of the change in interfacial tension. In order to allow a meaningful comparison, the interfacial tension isotherms for the two block terpolymers, SBT-2 and SBT-1, dissolved in cyclohexane, were determined at the immiscible phase boundary of water and cyclohexane. Upon addition of the block terpolymer to the cyclohexane solution the interfacial tension between cyclohexane and water is decreased from ca. 51 mN/m to ca. 30 mN/m. The determined interfacial tension of the pure cyclohexane/water system agrees well with the literature values.[32,33] The values for both block terpolymers are very close, and hence it can be concluded that the inner fraction of

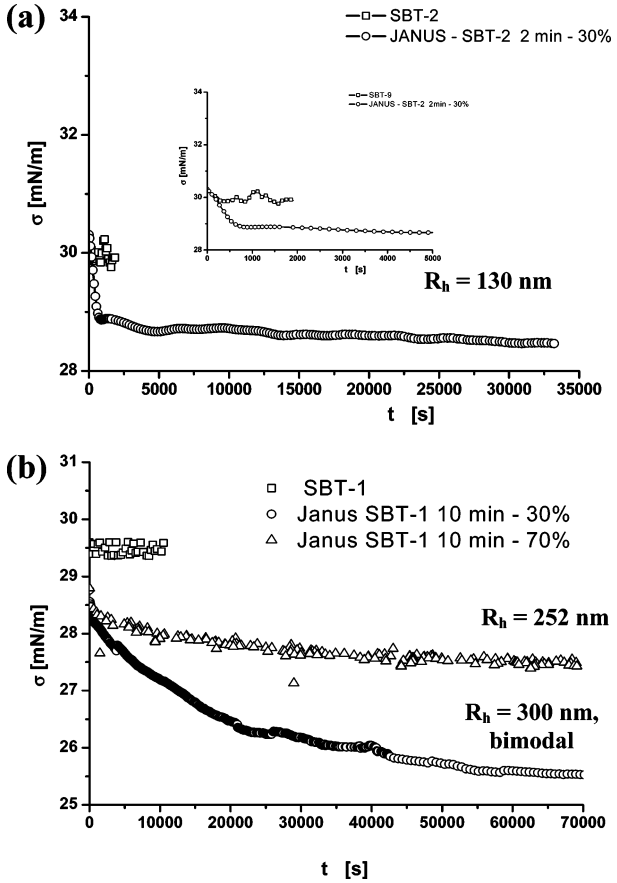

Figure 12. Interfacial tension isotherms of solutions of Janus discs in cyclohexane at the cyclohexane/water interface (c = 1 mg/mL). The isotherms of the block terpolymer precursors are shown for comparison. The *z*-average hydrodynamic radii of the samples investigated are shown within the diagrams and were obtained by DLS.

polybutadiene plays only a minor role for the reduction of the interfacial tension. In order to see an effect of the crosslinked architectures, the interfacial tension isotherms of the Janus discs are compared to the ones obtained for the block terpolymer solutions (Figure 12). A significant decrease of the interfacial tension of the system can be observed for all samples containing the Janus particles. For the SBT-1 based Janus discs two different samples are shown. The one with the higher hydrodynamic radius ($\langle R_h \rangle_z$ = 300 nm) possesses a bimodal size distribution, which is typically obtained at short sonication times (see above). It contains a fraction of relatively large flat Janus sheets ($R \approx 1-2\ \mu$m). On the contrary, the other sample shows a monomodal distribution; very large particles are not present in this case. It can be seen that the presence of larger particles leads to a stronger decrease of the interfacial tension, and thus it can be concluded that indeed the interfacial tension depends on the disc size. The lowest decrease of the interfacial tension can be found for the Janus disc sample based on the SBT-2 template, exhibiting the smallest particle size. The interfacial tension isotherms decay more slowly as compared to the pure block terpolymer isotherms. The observed decrease indicates that the systems are of a dynamic nature, as otherwise no long-lasting time-dependent change would be expected. After reaching the plateau value at longer time scales, the thermodynamically favored molecules should be placed and oriented at the interface. According to the theory of Nonomura et al.,[1] the largest discs adsorb most strongly.

(31) Glaser, N.; Adams, D. J.; Böker, A.; Krausch, G. *Langmuir* **2006**, *22* (12), 5227−5229.
(32) Landfester, K.; Willert, M.; Antonietti, M. *Macromolecules* **2000**, *33* (7), 2370−2376.
(33) d'Ans, J.; Lax, E. *Taschenbuch für Chemiker und Physiker*; Springer: Berlin, 1992.

The presented results of the effect of Janus discs on the interfacial tension of a liquid−liquid interface are remarkable, and one of the unique features predicted for disclike Janus particles, in particular, under the consideration that the particles themselves are only slightly amphiphilic. Even stronger changes are expected for strongly amphiphilic Janus discs. This novel class of particles is thus of high interest for studies concerning emulsion stabilization, technological formulations, or encapsulation of molecules.

3. Conclusions

We have been able to synthesize for the first time large sheetlike or disclike Janus particles, consisting of a crosslinked inner polybutadiene layer and two phase-segregated sides of polystyrene and poly(*tert*-butyl methacrylate). The particles can be obtained via a simple template-assisted approach, and their size can be tuned from the mesoscopic level to the nanometer scale, typically in the range of several micrometers to hundreds of nanometers. The size distribution of the Janus discs narrows progressively to moderate values with prolonged homogenization.

A detailed SFM investigation of these novel flat, brushlike polymeric nanoparticles has given a deep insight into the surface structures formed. The appearance of the particles adsorbed onto substrates is governed by a strong interplay between the brushlike behavior and the interfacial tensions of the system. Due to the introduced ultrasound energy, the sheetlike particles get "shaved" and exhibit circular disclike outer sides. By means of cryo-TEM, which was applied for the first time in THF, it was possible to visualize the aggregation behavior of the Janus discs *in situ*. The flat particles self-assemble into superstructures via back-to-back stacking even in good solvents. The aggregation into superstructures and the inherent multicompartment character of the structures could be demonstrated by embedding the Janus discs into a photo-crosslinkable silicon oil and subsequent direct TEM observation of the cross section after microtome cutting and staining. Finally, the effect of Janus discs on the interfacial tension of liquid−liquid interfaces (oil/water) was highlighted, serving as a model system for emulsion stabilization. The Janus particles show a distinct and significant decrease of the interfacial tension as compared to their linear uncrosslinked block terpolymer precursors and are therefore more efficient stabilizing agents. The decrease is most pronounced for the Janus discs with the largest diameters.

Acknowledgment. The authors would like to thank Georg Krausch, Robert Magerle, and Nicole Glaser for fruitful discussions as well as Thorsten Goldacker for the synthesis of SBT-2. Furthermore, we are indebted to Astrid Göldel and Clarissa Abetz for numerous TEM and SEM images. Felix Schacher is acknowledged for the microtome cutting. This work was supported by DFG within the ESF SONS-AMPHI Program and by the EU within the Marie Curie RTN POLYAMPHI. A.W. thanks the Bavarian Graduate Support Program for a scholarship.

Supporting Information Available: Experimental Part, NMR characterization, SFM images before annealing, evidence for back-to-back stacking by cryo-TEM and SFM, cryo-TEM images at low sonication times. This material is available free of charge via the Internet at http://pubs.acs.org.

JA068153V